Universality and scaling phenomenology of small-scale turbulence in wall-bounded flows

Liang Wei, Gerrit E. Elsinga, Geert Brethouwer, Philipp Schlatter, and Arne V. Johansson

Citation: Physics of Fluids (1994-present) **26**, 035107 (2014); doi: 10.1063/1.4868364
View online: http://dx.doi.org/10.1063/1.4868364
View Table of Contents: http://scitation.aip.org/content/aip/journal/pof2/26/3?ver=pdfcov
Published by the AIP Publishing

PHYSICS OF FLUIDS **26**, 035107 (2014)

Universality and scaling phenomenology of small-scale turbulence in wall-bounded flows

Liang Wei,[1,a)] Gerrit E. Elsinga,[2,b)] Geert Brethouwer,[1,c)]
Philipp Schlatter,[1,d)] and Arne V. Johansson[1,e)]
[1]*Linné FLOW Centre and Swedish e-Science Research Centre (SeRC), KTH Mechanics, SE-100 44 Stockholm, Sweden*
[2]*Laboratory for Aero and Hydrodynamics, Delft University of Technology, 2628CA Delft, The Netherlands*

(Received 23 September 2013; accepted 25 February 2014; published online 19 March 2014)

The Reynolds number scaling of flow topology in the eigenframe of the strain-rate tensor is investigated for wall-bounded flows, which is motivated by earlier works showing that such topologies appear to be qualitatively universal across turbulent flows. The databases used in the current study are from direct numerical simulations (DNS) of fully developed turbulent channel flow (TCF) up to friction Reynolds number $Re_\tau \approx 1500$, and a spatially developing, zero-pressure-gradient turbulent boundary layer (TBL) up to $Re_\theta \approx 4300$ ($Re_\tau \approx 1400$). It is found that for TCF and TBL at different Reynolds numbers, the averaged flow patterns in the local strain-rate eigenframe appear the same consisting of a pair of co-rotating vortices embedded in a finite-size shear layer. It is found that the core of the shear layer associated with the intense vorticity region scales on the Kolmogorov length scale, while the overall height of the shear layer and the distance between the vortices scale well with the Taylor micro scale. Moreover, the Taylor micro scale collapses the height of the shear layer in the direction of the vorticity stretching. The outer region of the averaged flow patterns approximately scales with the macro scale, which indicates that the flow patterns outside of the shear layer mainly are determined by large scales. The strength of the shear layer in terms of the peak tangential velocity appears to scale with a mixture of the Kolmogorov velocity and root-mean-square of the streamwise velocity scaling. A quantitative universality in the reported shear layers is observed across both wall-bounded flows for locations above the buffer region. © *2014 AIP Publishing LLC*. [http://dx.doi.org/10.1063/1.4868364]

I. INTRODUCTION

Turbulent flows are usually characterized by a broad range of scales; the higher the Reynolds number, the broader the range of scales. Large scales are flow dependent, but small scales show universal characteristics in general. This universality has led to the development of turbulence modeling approaches like large-eddy simulation (LES). The study of small-scale turbulence is of great theoretical and practical importance. It may contribute to a proper theory of turbulence, vortex dynamics, combustion/turbulence mixing, turbulence modeling, and propagation of light and sound waves.[1] The aim of the present work is to investigate the universal structures of small-scale turbulence motions and their Reynolds-number scaling for different types of wall-bounded turbulent flows.

[a)]Electronic mail: wei@mech.kth.se
[b)]Electronic mail: G.E.Elsinga@tudelft.nl
[c)]Electronic mail: geert@mech.kth.se
[d)]Electronic mail: pschlatt@mech.kth.se
[e)]Electronic mail: johansson@mech.kth.se

Many studies have been done to discover and understand the universal features of small-scale turbulent motions. Kerr[2] studied high-order derivative correlations and alignment of small-scale structures in direct numerical simulation (DNS) of isotropic turbulence. Simulations were conducted on up to 128^3 grid points with periodic boundary conditions to achieve Reynolds numbers up to 82.9 based on Taylor micro scale. It was concluded that the vorticity is concentrated in tubes (see also She *et al.*[3]) with regions of intense strain nearby. The largest principal rate of strain was negative or compressive because the velocity-derivative skewness was negative. Both the largest compressing and stretching components of the rate of strain were oriented perpendicular to the tube, while the weak stretching component (the intermediate eigenvector of the strain rate tensor) was aligned along the tube, that is, there was a preferential alignment of the vorticity vector with the intermediate strain direction. This alignment was further investigated by Ashurst *et al.*[4] using the DNS data of isotropic turbulence[2] and homogeneous shear flow.[5] They confirmed the alignment and argued that it was a consequence of angular momentum conservation. Jiménez[6] offered another explanation for the alignment using a kinematic model and attributed it to purely kinematic effects. There have been many more studies about the vorticity alignment,[7–13] considering various flows like isotropic turbulence, turbulent channel flow (TCF), turbulent boundary layer (TBL), atmospheric turbulence, and magnetohydrodynamic turbulence.

Vorticity and strain-rate eigenvectors are linked to turbulence structures. Many researchers have investigated the shape and alignment of various type of turbulence structures using different methods.[4,14–19] Some observed a 10°–20° inclination angle of the turbulence structures with the wall/streamwise direction in shear flow using space-time streamwise velocity correlations and wall shear stress, conditionally averaged isocontours of the normalized disturbance streamwise velocity,[14,16,19] while some others observed 45° inclination angle by means of vorticity, smoke lines, and temperature fronts.[15,17,18] It appears that different quantities may exhibit different kinds of structures. Ashurst *et al.*[4] explained that not all tube-like concentrated vorticity adopted the 45° hairpin shape, e.g., for flows driven by irrotational strain, vortex tubes were also aligned with the positive strain direction, but the hairpin shape would not appear without the mean shear.

Besides the alignment of vorticity and structures, flow topology was another focus of small-scale turbulence studies. Chong *et al.*[20] proposed a topology classification for three-dimensional flow fields using tensor invariants P, Q, R, in which four different regions were categorized in the Q-R space ($P = 0$ for incompressible flow). Blackburn *et al.*[21] studied these fine-scale motions in TCF and showed that the joint probability-density function (pdf) of Q-R has a teardrop shape further away from the wall, and confirmed the alignment of the vorticity vector and the intermediate eigenvector of the strain-rate tensor. In addition to the kinematics of the flow, the dynamics of turbulence flow topology was also studied. Elsinga and Marusic[22] experimentally investigated the dynamics of flow topology in the outer layer of a TBL. It was found that both the instantaneous joint pdf of Q-R and their average temporal behavior was in agreement with the local flow topology in DNS of isotropic turbulence, as in Ooi *et al.*[23] The lifetime of the energy-containing eddies was determined by the period of the orbit in the Q-R phase plane, where the topology evolutions described spiraling orbits and tended to converge to the origin, which could be translated into a cyclical variation of the flow topology. Elsinga and Marusic[12] proposed a method to extract average flow patterns around a point in a local frame of reference defined by the eigenvectors of the strain rate tensor and applied the method to three turbulent flow cases: a TBL, a TCF, and homogeneous isotropic turbulence. The statistics were mainly collected in the regions around $0.2h$ away from the wall (h is the boundary layer thickness/half channel width) for TBL and TCF. It was found that for all three cases the average pattern showed a shear layer structure separating two larger-scale, relatively uniform regions. The vorticity alignment and the tear-drop shape of the pdf of the velocity gradient invariants Q-R were further analyzed.

Indeed, instantaneous structures of that kind have also been observed. Meinhart and Adrian[24] have shown the existence of (nearly) uniform momentum zones in a boundary layer, which are bounded by thin layers containing vortical motions. These layers can be regarded as shear layers due to the velocity difference across them. These observations have been detailed further in Adrian *et al.*[25] Additionally, Del Álamo *et al.*[26] have estimated the fractal dimension of vortex clusters in the logarithmic region to be 2, which suggests again an organization of vortices on surfaces or sheets.

The Reynolds number has a great effect on turbulence motions, especially the size of the smallest scales. Turbulent flows with a broad range of Reynolds numbers are needed for a further study of the universality of small-scale turbulence motions. The current work uses the averaging scheme proposed by Elsinga and Marusic[12] (with slightly different local coordinate systems) in the strain-rate eigenframe to investigate the universality and scaling phenomenology for TBL and TCF at different Reynolds numbers and different distances to the wall. One important difference between TBL and TCF is that the former exhibits a large degree of intermittency in the outer region.[27] This study is focused on the turbulence-dominated regions.

II. METHODOLOGY

The current study aims at investigating the universality among statistically steady flows (TCF and TBL) at different Reynolds numbers and wall normal locations. The focus is its kinematics instead of dynamics which is beyond the scope of the current study. Therefore, the flow field is evaluated statistically, by using the principal strain-rate eigenframe of reference. The main reason is that this frame of reference is associated with some universal features of small-scale turbulence like the preferential alignment between the vorticity vector $\boldsymbol{\omega}$ and the intermediate principal straining direction, and in addition, the invariants of the velocity gradient tensor (Q, R) are also linked, in part, to principal straining.[12]

The strain-rate tensor, $S_{ij} = 0.5 * (\partial v_i/\partial x_j + \partial v_j/\partial x_i)$, where v_i is the ith velocity component, can be diagonalized. This diagonalized tensor has three eigenvalues ($\lambda_1 > \lambda_2 > \lambda_3$) and respective three eigenvectors ($\boldsymbol{\lambda}_1$, $\boldsymbol{\lambda}_2$, and $\boldsymbol{\lambda}_3$), which are orthogonal due to the symmetry of S_{ij}. For incompressible flows $\lambda_1 > 0$ and $\lambda_3 < 0$ since the sum of the eigenvalues is zero. $\boldsymbol{\lambda}_1$ and $\boldsymbol{\lambda}_3$ represent the most stretching and compressing directions, respectively. The direction of $\boldsymbol{\omega}$ at different points in a flow field is different, but it is often aligned with $\boldsymbol{\lambda}_2$, as shown by many studies.[4,6,12,21] If the flow field around each point is mapped along the local $\boldsymbol{\lambda}_1$, $\boldsymbol{\lambda}_2$, $\boldsymbol{\lambda}_3$ directions, a local flow field is obtained as it is viewed from an observer aligned with the local eigenframe. We may expect to see some common features associated with the local strain field and it is interesting to investigate their statistical structures both qualitatively and quantitatively.

The method to collect point-wise statistics in the local strain-rate eigenframe applied in this study consists of the following steps (see Figure 1 for a 2D illustration): (1) Choose a specified subdomain (G) in the turbulent region of the flow field. (2) Compute $\boldsymbol{\lambda}_1$, $\boldsymbol{\lambda}_2$, and $\boldsymbol{\lambda}_3$ of $\boldsymbol{S}_{ij}$ at one point, e.g., A. The $\boldsymbol{\lambda}_3$ direction is adjusted to maintain a right-handed system, after $\boldsymbol{\lambda}_2$ and $\boldsymbol{\lambda}_1$ are fixed (Note that the principal straining axes do not have positive directions defined. Therefore one may define positive directions, for instance, based on the vorticity vector $\boldsymbol{\omega}$ and the streamwise

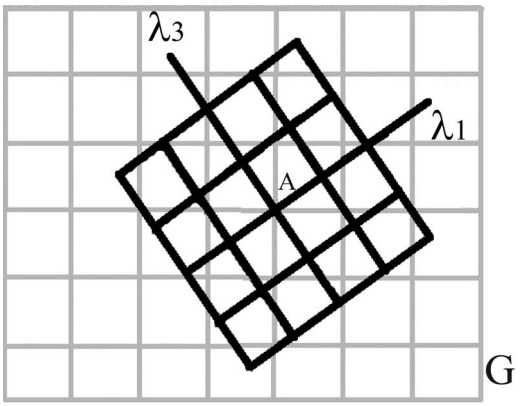

FIG. 1. For simplicity, a 2D illustration of the local grid ($\boldsymbol{\lambda}_1$, $\boldsymbol{\lambda}_3$) at the point A (black lines), and the global grid (gray lines) within a selected subdomain G (e.g., a small fraction of the flow field). Note that a global grid beyond G may be used when the points near the edge of G are considered. G can be seen as the collection of all points A over which the averaging is performed. For TCF, G is just a single x-z plane. For TBL, G extends between 0.22 and 0.38δ.

$\boldsymbol{x}$-direction). $\boldsymbol{\lambda}_2$ is chosen so that the angle between $\boldsymbol{\lambda}_2$ and $\boldsymbol{\omega}$ is positive, the same as Elsinga and Marusic.[12] The difference is that here $\boldsymbol{\lambda}_1$ is aligned with the positive $\boldsymbol{x}$ direction (the dot product of $\boldsymbol{\lambda}_1$ and $\boldsymbol{x}$ is positive) since it seems appropriate to see the stretching of vortices in the streamwise direction for wall-bounded flows. This specific choice of alignment will be most importantly close to the wall where the turbulence is strongly anisotropic. Conversely, negligible effects were seen in the near-isotropic regions further away from the wall. (3) Create a uniform grid in the local coordinate system originated at A with three principal directions along $\boldsymbol{\lambda}_1$, $\boldsymbol{\lambda}_2$, and $\boldsymbol{\lambda}_3$. This local mesh extends at least $0.5\,h$ in all directions (where h is the half channel width for TCF and the boundary layer thickness δ for TBL). (4) Map the global fluctuating velocity field around A onto the local uniform grid to get the local velocity field. (5) Apply steps 2–4 to all points in the subdomain (G) and average the obtained local velocity fields over the local grid to get the averaged three-dimensional flow patterns.

III. RESULTS AND ANALYSIS

The databases used in the current study are from DNS of fully developed TCF with friction Reynolds numbers up to $Re_\tau \approx 1500$, and a spatially developing, zero-pressure-gradient TBL with the Reynolds number up to $Re_\theta \approx 4300$ ($Re_\tau \approx 1400$), based on the momentum thickness θ and free-stream velocity.[28,29] For comparison and scaling purpose, the Reynolds numbers considered for the current cases are $Re_\tau \approx 550$, 1000, 1500 and 550, 1000, 1350 for TCF and TBL, respectively, and the specified subdomain considered for both type of flows is around $0.3h$, well in the outer region, more specifically, $0.3h$ for TCF, and 0.22-0.38δ for TBL, where turbulence dominates and boundary layer intermittency is negligible. Some related results will be discussed in Sec. III B. In addition, different regions in the wall-normal direction (viscous sublayer, buffer layer, log layer) are also considered for two channel flow cases to examine the application range of the universality, which will be presented in Sec. III C.

A. Local coordinate and flow topology

The creation of the local coordinate based on the strain-rate eigenvector in this study involves the alignment of $\boldsymbol{\lambda}_2$ with $\boldsymbol{\omega}$ and the alignment of $\boldsymbol{\lambda}_1$ with the positive streamwise direction $\boldsymbol{x}$ in order to make the local coordinate unique. First, it is interesting to know how the local coordinates are oriented in different regions of the flow. Figure 2 presents the pdf of the cosine of the angle θ between $\boldsymbol{\lambda}_2$ and $\boldsymbol{\omega}$, and between $\boldsymbol{\lambda}_1$ and the wall-normal $\boldsymbol{y}$ direction, for TCF at $Re_\tau \approx 550$ in four different regions: viscous sublayer, buffer layer, log layer, and wake region. It can be seen that the profiles for the alignment between $\boldsymbol{\lambda}_2$ and $\boldsymbol{\omega}$, shown in

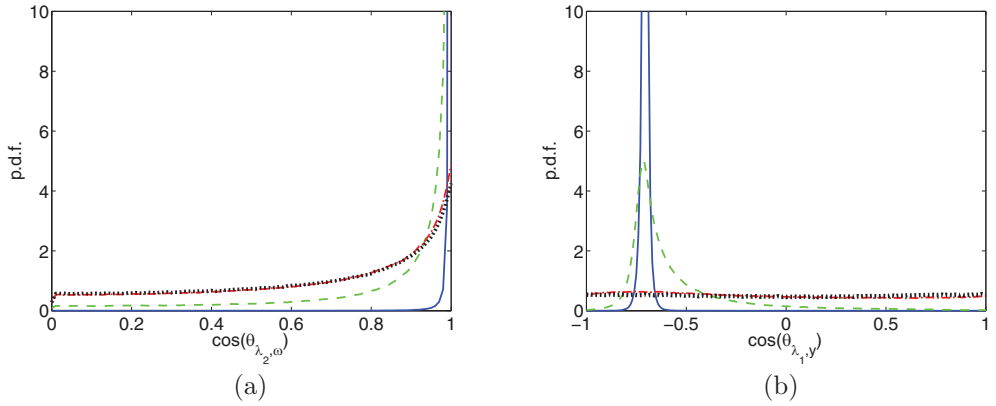

FIG. 2. pdf of the angle between λ_2 and ω (a), and between λ_1 and y (b) for TCF at $Re_\tau = 550$. The various lines correspond to $y^+ = 4$ (solid line), 16 (dashed line), 153 (dashed-dotted line), 534 (dotted line), corresponding to the viscous sublayer, buffer layer, log layer, and wake region, respectively.

Figure 2(a), peak at $\theta = 0$ for all regions. The closer to the wall, the better the alignment. Similar results are found for other Reynolds numbers and boundary layers (not shown here), and these results are in good agreement with the findings of Blackburn *et al.*[21] In the viscous sublayer $\boldsymbol{\lambda}_2$ and $\boldsymbol{\omega}$ are almost perfectly aligned as for a shear layer. The alignment between $\boldsymbol{\omega}$ and the spanwise direction (z), and between $\boldsymbol{\lambda}_2$ and z very near the wall was confirmed by previous work[18] and the current one (not shown here), respectively.

The alignment of strain-rate eigenvectors with the global coordinates (e.g., $\boldsymbol{y}$ shown in Figure 2(b)) shares some common features: strong alignments are seen in the viscous sublayer and buffer layer, but no preferable alignment in the log layer and wake region. It is also observed that in the viscous sublayer and buffer layer, both $\boldsymbol{\lambda}_1$ and $\boldsymbol{\lambda}_3$ (not shown here) have an angle of 45° inclined with $\boldsymbol{y}$ direction and point away from the wall, but the difference is that $\boldsymbol{\lambda}_1$ is pointing downstream while $\boldsymbol{\lambda}_3$ is pointing upstream. These orientations correspond to the $\boldsymbol{\lambda}_1$ and $\boldsymbol{\lambda}_3$ directions of a pure shear layer. The same orientations are seen for the other cases.

Now the local coordinate system, defined by $\boldsymbol{\lambda}_1$, $\boldsymbol{\lambda}_2$, and $\boldsymbol{\lambda}_3$, is employed to compute the averaged flow patterns as explained in Sec. II. Like the alignment, the averaged flow patterns in the local strain-rate eigenframe are similar for all cases. For simplicity, only the results of TCF at $Re_\tau \approx 550$ and TBL at $Re_\tau \approx 1000$ are shown here. Figure 3 presents the averaged fluctuating velocity vector field in three different cross planes. Coordinates are normalized using the Kolmogorov scale. Two vortical regions with the same sense of rotation embedded in a shear layer can be seen in the vector field plot on the plane where $\lambda_2 = 0$ (λ_1-λ_3 plane), as shown in Figure 3(a). The scaling of this structure will be discussed later in this section. Figures 3(c) and 3(e) present the vector plots at $\lambda_3 = 0$ and $\lambda_1 = 0$ planes, respectively. The stretching in the $\boldsymbol{\lambda_1}$ direction and compression in the $\boldsymbol{\lambda}_3$ direction are obvious. The vectors also indicate a weak stretching in the $\boldsymbol{\lambda}_2$ direction. The shear layer and in particular the two vortices weakly stretched in the λ_2 direction are more clearly seen in a visualization of the three-dimensional streamlines of the averaged flow pattern shown in Figure 4. As already discussed in the Introduction, this averaged flow has a strong resemblance to instantaneous structures observed in wall-bounded shear flows.[24,26] For a more extensive discussion of a connection to instantaneous flow we refer to Elsinga and Marusic.[12] Figures 3(b), 3(d) and 3(f) show flow patterns for TBL at $Re_\tau \approx 1000$, which are similar to the ones in Figures 3(a), 3(c), and 3(e), especially close to the origin. The slight difference in magnitude between the two cases further away from the origin is mainly due to the Reynolds number effects. Patterns in this region represent scales somewhere between small and large scales. The related Reynolds number scaling and physics will be further discussed in Sec. III B.

The flow topology is computed from the averaged flow patterns using the invariants of the velocity gradient tensor Q-R. It can be classified into four different quadrants in the Q-R plane.[20,21] The flow patterns in Figure 3 mainly fall into two categories: stable focus/stretching, and unstable node/saddle/saddle, as confirmed by the joint pdf of Q-R in Figure 5. The contour lines exhibit the expected teardrop shape for both TCF and TBL, a typical feature of small-scale turbulence in many different types of flows.

The above discussions about the universality of the averaged flow patterns were so far mainly conducted in a qualitative way. A quantitative study is needed for further evaluating the universality. The averaged flow field has patterns related to flow topology and turbulence scales on which Reynolds number has a significant effect. It is interesting to investigate this effect which may shed some light on turbulence modeling, e.g., sub-grid scale models for large-eddy simulation (LES).

B. Reynolds-number scaling of the averaged flow patterns

Reynolds-number scalings of the universal flow patterns for all cases are computed using the Kolmogorov (length η and velocity u_η) and Taylor scales ($l_t = \sqrt{\overline{u^2}/\overline{u_x^2}}$, where $\overline{u^2}$ is the mean streamwise turbulence intensity and $u_x = \partial u/\partial x$), and the macro scale ($h$). Close to the origin, Kolmogorov or Taylor scalings may be expected, but further away from the wall, neither of these two scalings is probable and the macro scale may be depending on the size of scales. Since the local flow pattern indicates a shear layer with two vortical regions, as indicated in Figure 3(a), the scalings

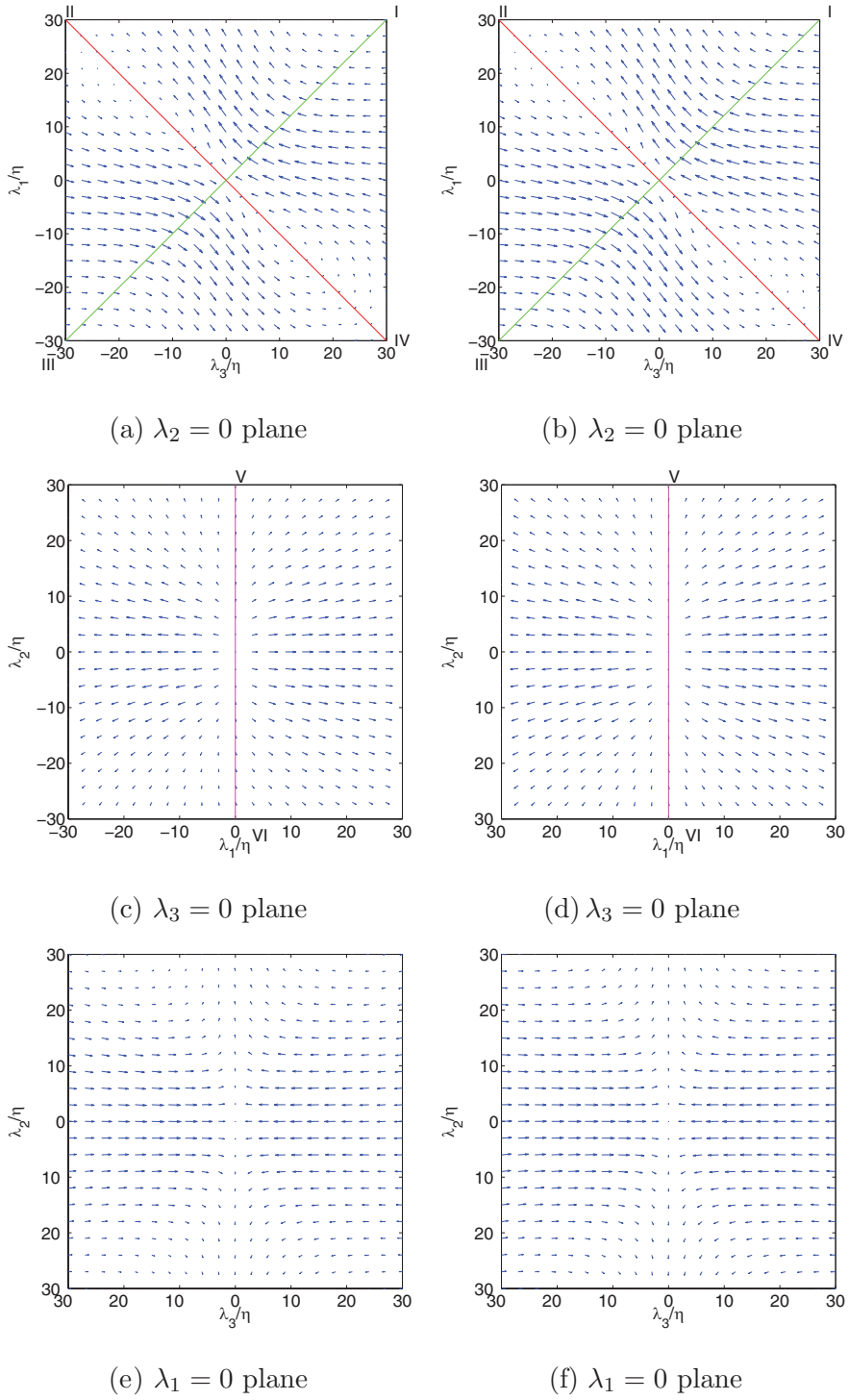

(a) $\lambda_2 = 0$ plane (b) $\lambda_2 = 0$ plane

(c) $\lambda_3 = 0$ plane (d) $\lambda_3 = 0$ plane

(e) $\lambda_1 = 0$ plane (f) $\lambda_1 = 0$ plane

FIG. 3. Averaged fluctuating velocity field in the local strain-rate eigenframe for TCF at $Re_\tau \approx 550$ ((a), (c), (e)) and for TBL at $Re_\tau \approx 1000$ ((b), (d), (f)). Axes are scaled with the Kolmogorov length scale η. Lines I, II,..., IV in ((a), (b)) and V, VI in ((c), (d)) are used for the velocity profiles below.

will be focused on their parameters, such as the thickness, width, strength of the shear layer, and the distance between the two vortical regions, which will be discussed below.

The thickness and strength of the shear layer in Figure 3 are determined from the profiles of the velocities along lines I and III in Figure 3(a) with their origin located at the center ($\lambda_3 = \lambda_1$

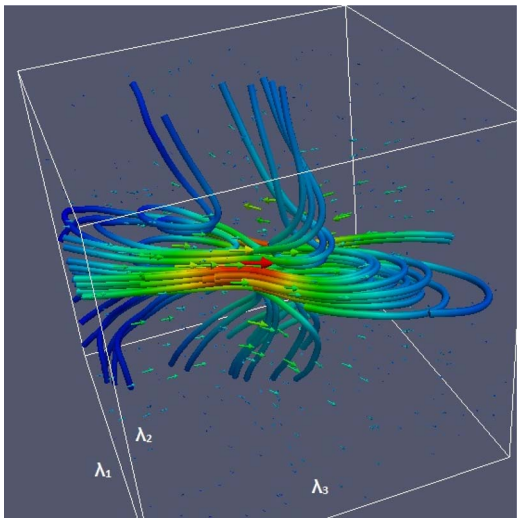

FIG. 4. 3D streamlines in the local strain-rate eigenframe, with the origin located in the center of the cube. Colors from blue to red represent increasing velocity magnitude.

$= \lambda_2 = 0$). The related Reynolds-number scalings using Kolmogorov length scale, Taylor micro scale, and macro scale are generated for both lines I and III and both profiles are very close to rotational symmetry due to quasi-homogeneity. Therefore, the profiles over lines I and III are averaged for presentation purposes (similar averaging procedures are done for the scaling profiles of the other pairs: lines II-IV, V-VI, in this section) and plotted in Figure 6, where λ_{45} is defined along the direction of line I-III and u is the shear velocity, that is, the velocity component perpendicular to the line I-III. It can be seen that Kolmogorov scaling profiles lead to a fairly good collapse of the profiles until reaching the peak of the velocity at $\lambda_{45} \approx 9\eta$ while Taylor scaling appears more appropriate away from the origin. In particular, the Taylor length scale seems to mark the transition from the shear velocity peak to an "outer" tail, in which point can be defined as the total thickness of the shear layer. The scalings give a total shear layer thickness of around $1l_t$. The shear layers share a universal thickness for both TCF and TBL, as can be seen in Figures 6(a) and 6(b). The quantitative

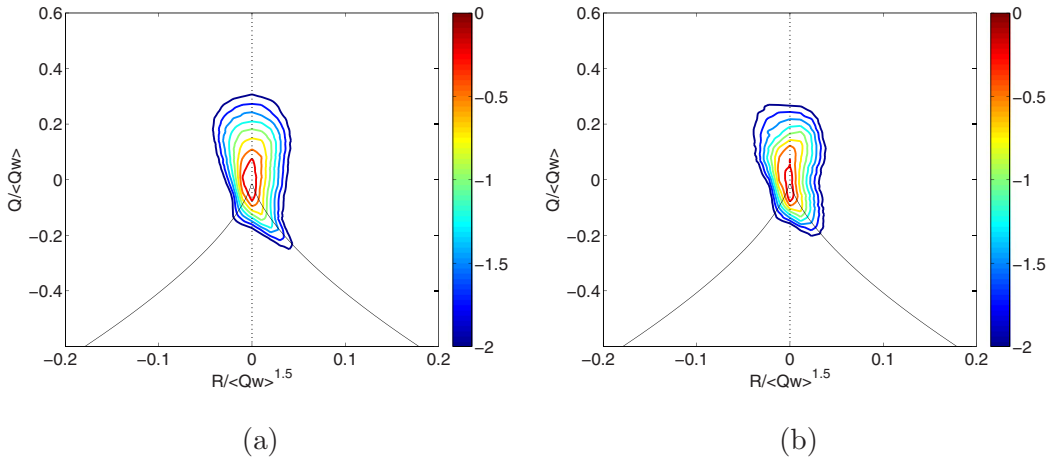

FIG. 5. Normalized joint pdf of Q-R for TCF at $Re_\tau \approx 550$ (a) and TBL at $Re_\tau \approx 1000$ (b) in the local strain-rate eigenframe. Q_W is the second invariant of the rotation-rate tensor. The thinner black solid line represents the zero-discriminant: $D = 27/4R^2 + Q^3 = 0$, which separates the four quadrants together with the dotted line $R = 0$. The contour levels have a log-scale distribution.

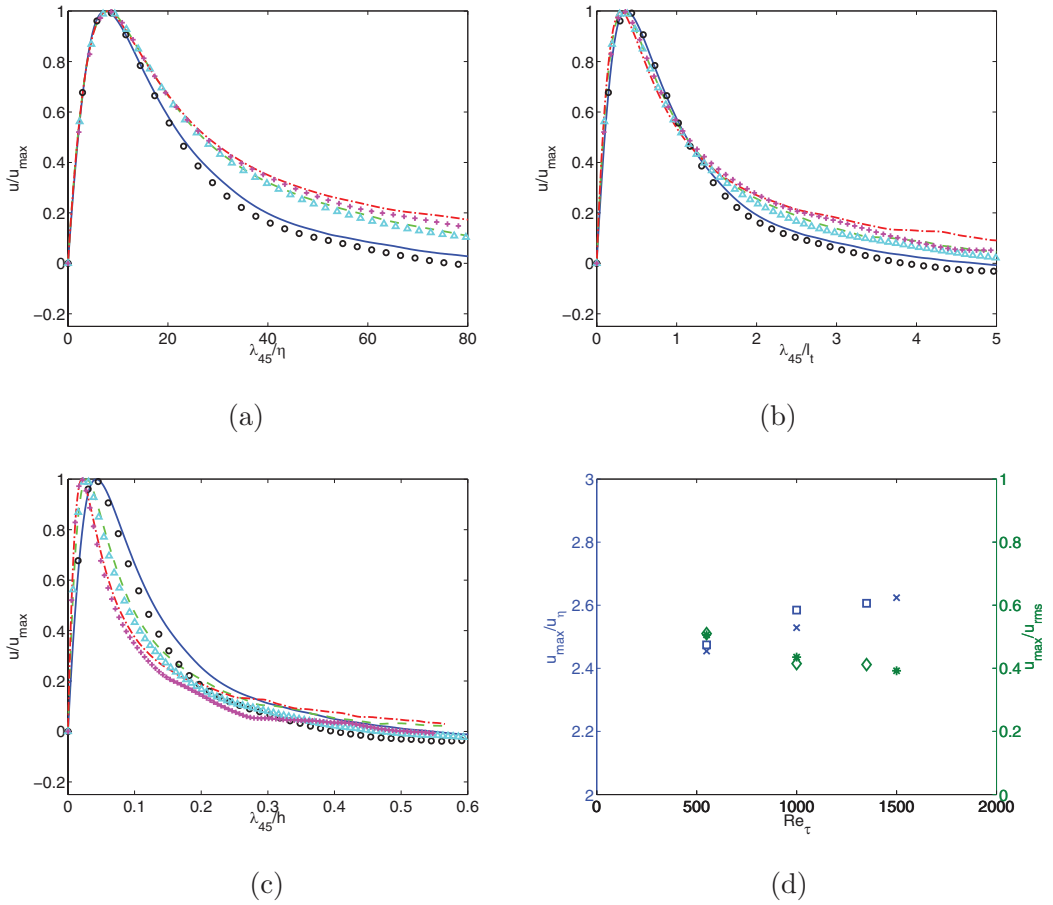

FIG. 6. Scaling of the shear layer using Kolmogorov length scale η (a), Taylor micro scale l_t (b), macro scale h (c), and related peak velocity scalings using Kolmogorov velocity scale u_η and root-mean-square of the streamwise velocity u_{rms} (d), where λ_{45} ($\lambda_{45} = \lambda_3/\cos(\pi/4)$) is on line I-III in Figure 3(a) and u is on and perpendicular to line I-III, u_{max} is the maximum velocity, h is the half channel width/boundary layer thickness. The various lines and symbols correspond to TCF at $Re_\tau = 550$ (solid line), 1000 (dashed line), 1500 (dashed-dotted line), TBL at $Re_\tau = 550$ (circles), 1000 (triangles), 1350 (plus), and peak velocity for TCF scaled by u_η (cross), u_{rms} (star) and for TBL scaled by by u_η (square), u_{rms} (diamond), the same hereafter in this section.

universality extends up to about $1l_t$, after which the profiles start to deviate. Moreover, the tail is seen to increase with Reynolds number consistent with the largest scales increasing in size when expressed in Taylor length scales. In particular, the tail seems flow dependent, as expected for large scales. The curves approach zero at approximately the same length scaled in outer units (Fig. 6(c)), illustrating the influence of large outer scales. This scaling is further improved if u_{rms} is used as normalization of the velocity. Here the peak location is moving closer to the origin with increasing Reynolds number, which is an indication of increased scale separation.

In addition to the length scalings discussed above, velocity scalings using u_η and u_{rms} are also analyzed. Only the scaling of the peak velocity u_{max} is plotted for simplicity and shown in Figure 6(d). It can be seen that the peak velocity is around $2.5u_\eta$ or $0.4u_{rms}$ for both TCF and TBL. Yet both u_{max}/u_η and u_{max}/u_{rms} vary slightly with Reynolds number, which indicates a mixed scaling of the shear layer strength containing small (u_η) and large scale (u_{rms}) influences simultaneously. Differences between TCF and TBL are small, and therefore not only the thickness of the shear layer but also its strength are quantitatively universal.

The distance between the two vortices in the shear layer is another important fundamental feature of the structure. It can be obtained through the profiles of velocities perpendicular to line II-IV in Figure 3(a). The Kolmogorov, Taylor and macro length, and velocity scaling pro-

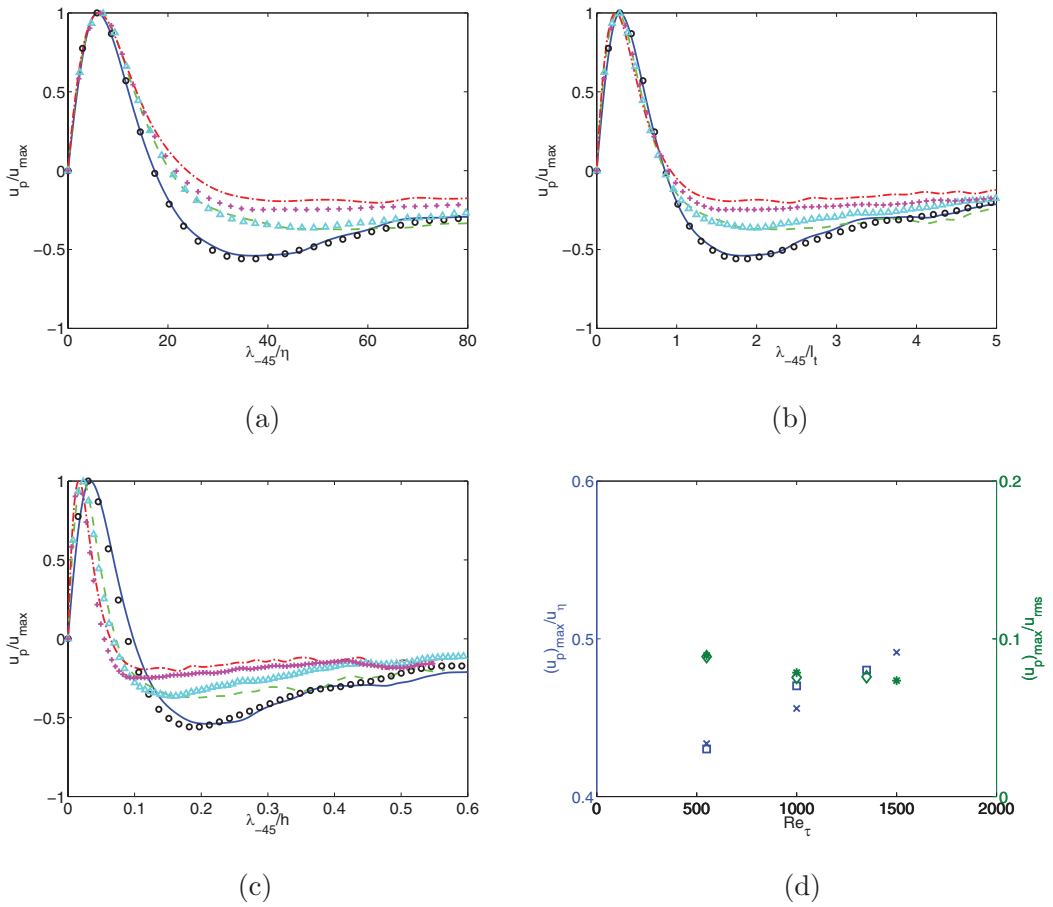

FIG. 7. Scaling of the vortex velocity profile using η (a), l_t (b), h (c), and the scaling of the peak velocities using u_η and u_{rms} (d), where $\lambda_{-45} = \lambda_1/\cos(\pi/4)$ on line II-IV in Figure 3(a) and u_p represents the velocity perpendicular to line II-IV, that is, perpendicular to the shear layer.

files are compared in Figure 7. The peak and zero-crossing of the velocity profiles approximately represent the edge and center of the vortex, respectively. The results indicate that the edge location is $\lambda_{-45} \approx 7\eta$ or $0.28l_t$ (Figures 7(a) and 7(b)) with an edge velocity of $0.5u_\eta$ or $0.08u_{rms}$ (Figure 7(d)), which is about 1/5 of the peak velocity in the shear layer, and the center of the vortex is at $\lambda_{-45} \approx 0.82l_t$. This gives a distance of around $1.64l_t$ between the cores of two vortices for all cases, which is similar to the spacing of $1.7l_t$ reported by Elsinga and Marusic.[12] The scaling profiles based on the Taylor scale seem to have a slightly better collapse between the cores of two vortices. Interestingly, a Reynolds number dependence is seen in the tails of Kolmogorov and Taylor scaling profiles. As an indication of large scales, all the macro scaling profiles have returned to zero beyond $0.5h$, which shows the extent of the shear layer. The velocity scalings shown in Figure 7(d) look similar to Figure 6(d). It seems that both velocity scalings show a slight (positive and negative) trend, suggesting a mixed scaling for the current cases, but higher Reynolds number cases will be needed to draw a firm conclusion about the velocity scalings.

Now scalings of some characteristics of the averaged shear-layer patterns in the $\lambda_2 = 0$ plane including shear layer thickness, strength, vortex distributions, and the horizontal span are discussed. The vertical span, or the height of the shear layer along the $\boldsymbol{\lambda}_2$ direction, i.e., the direction aligned with the vorticity vector is of interest to determine the extent of the shear layer and to complement the study of the local 3D flow structure. One way is to compute the shear strength, i.e., the derivative of shear velocity $\partial u/\partial\lambda_{45}$, along $\boldsymbol{\lambda}_2$ (along line V-VI in Figure 3(c)), as displayed in Figure 8. It can be seen that it scales well with Taylor scale. Defining the outer edge as the position where the

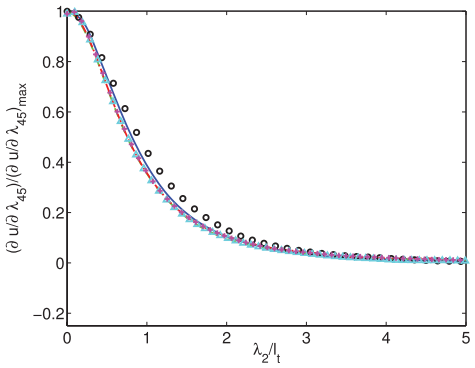

FIG. 8. Scaling of shear layer height in the λ_2 direction, i.e., $\frac{\partial u}{\partial \lambda_{45}}$, on line V-VI in Figure 3 using l_t, where u is the same shearing velocity shown in Figure 6.

velocity is half of its maximum value, gives a universal height of around $1.6l_t$ (taking into account symmetry).

It can be seen from the above discussions that the different parts of the obtained shear-layer like structure scale on Kolmogorov, Taylor, and the macro scale, which indicates that the structure represents both small and large scales of turbulence. Kolmogorov scaling performs well near the origin, where viscosity seems important, and Taylor scale appears to give a good collapse in a broader region, while macro length scaling works well further away from the origin, i.e., outside the shear layer. The universal structure of the shear layer indicates a thickness of around $1l_t$ separating large scale motions and a common height of around $1.6l_t$ for the current cases with the current subdomain located in the outer layer at around $0.3h$ away from the wall. The two aligned vortices inside the layer are spaced $1.6l_t$ apart. The scaling at other locations will be discussed in Sec. III C.

C. Wall–normal scaling of the averaged flow patterns

It was discussed in Sec. III B that the averaged flow patterns for TCF and TBL in the local strain-rate eigenframe with a specified subdomain chosen as the region around $0.3h$ away from the wall appear universal when applying an appropriate scaling. It is interesting to see how universal it is for the subdomain in the regions closer to the wall. Scaling profiles at different wall-normal locations for different cases are thus considered next. Since the profiles for different cases (Reynolds number, flow case) were similar, only those for the $Re_\tau = 1000$ channel flow case are presented here.

The wall-normal locations considered are $y^+ = 12$, 50, 169, 299 in wall units. The closest location $y^+ = 12$ is in the buffer layer and the furthest one $y^+ = 299$ is at $0.3h$ for the current case, that is, on the edge of the log-law region and the wake region.[30] Taylor and macro length scalings of the shear layer and distance between the vortices are presented in Figure 9. To obtain the profiles for the locations $y^+ = 50$–299 the same averaging procedure as before for lines I-III and II-IV has been applied since the flow field in the strain-rate eigenframe is nearly homogeneous. At $y^+ = 12$ only the profiles on line I and II are shown in Figures 9(a) and 9(b), respectively, because the flow near the wall is strongly inhomogeneous and the eigenframe has a clear preferential orientation, as discussed in Sec. III A. The averaged flow field at all wall-normal locations displays a clear shear layer structure with a Kolmogorov scaling of the inner part as expected (not shown here). However, the two aligned vortices are only observed in the averaged flow fields above the buffer layer at $y^+ = 50 - 299$, see Figure 9(b). The averaged flow patterns at these locations show strong similarities with a Taylor micro scaling of the size of the shear layer and distance between the vortices, see Figures 9(a) and 9(b), respectively.

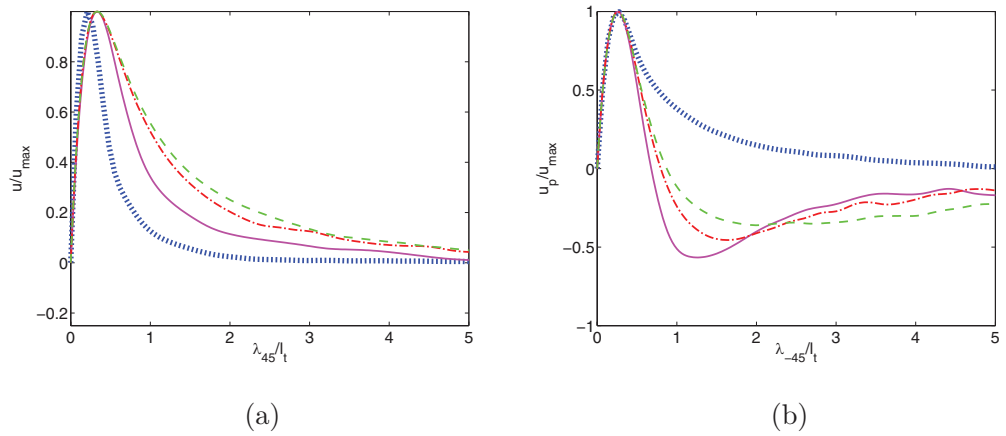

FIG. 9. Scaling of the shear layer (a) and the distance between vortices (b) for $Re_\tau = 1000$ TCF at different wall-normal positions, using l_t. The various lines and symbols correspond to different wall normal locations $y^+ = 12$ (dotted line: scaling on line I or II in Figure 3), 50 (solid line), 169 (dashed-dotted line), 299 (dashed line).

IV. CONCLUSIONS

The universality of small-scale turbulence motions in well-resolved spectral DNS data of turbulent channel and boundary-layer flow at different Reynolds numbers and various wall normal locations has been investigated using the average flow pattern in the eigenframe of the strain-rate tensor. The related Reynolds-number scaling has been considered for friction Reynolds numbers between 550 and 1500. The applied methodology is to map a global flow field around a point in some chosen subdomain onto a local coordinate defined by the eigenvectors of the strain-rate tensor, in order to obtain a local flow field, and average these local flow fields for all points in the subdomain to get a statistically averaged flow pattern. Using this approach, the small-scale structure of the flow field and the dimensions of this structure can be studied quantitatively and systematically.

Above the buffer layer at $y^+ = 50$ and beyond, the resulting average flow patterns in TBL and TCF feature a distinct shear layer containing two aligned vortices, in agreement with previous work that showed a similar structure in the outer layer of TBL, TCF, and isotropic turbulence.[12] The vorticity inside the shear layer is being stretched in the direction of the intermediate principal strain. The joint pdf of the invariants Q and R of this structure has the same characteristic teardrop shape as that of the non-averaged flow field, showing that the applied methodology captures the fundamental features of the small-scale turbulence. The average flow pattern near the wall in the buffer layer also reveals a shear layer but no clear evidence of vortices indicating that the small-scale flow field is dominated by shear near the wall.

For the first time, the structures in the strain-rate-eigenframe have been studied in a quantitative way by considering the scaling of the profiles across and along the shear layer. We find that above the buffer layer, in the log layer and wake region, the thickness and span of the shear layer and the distance between the two vortices scales well with the Taylor micro scale in all cases. Only the innermost part of the shear layer displays a clear Kolmogorov scaling while the outermost part suggests a macro scaling. The intensity of the shear layer appears to obey a mixed scaling based on the Kolmogorov velocity scale and u_{rms}. Although we focused on the small scales in this study by conditioning on the local velocity gradients and local principal strain directions, we see thus clear indications of the direct influence of large scales on small-scale motions in both velocity and length scalings. In summary, a high degree of universality of the small scale motions is demonstrated quantitatively through this scaling of the structures defined in the strain-rate-eigenframe of reference.

ACKNOWLEDGMENTS

The authors would like to thank KTH Royal Institute of Technology for the funding support. SNIC (Swedish National Infrastructure for Computing) is acknowledged for providing computing

resources. We acknowledge PRACE (Partnership for Advanced Computing in Europe) for awarding us via the REFIT project access to resource *Jugene* at the Jülich Supercomputing Centre in Germany.

[1] K. R. Sreenivasan and R. A. Antonia, "The phenomenology of small-scale turbulence," Annu. Rev. Fluid Mech. **29**, 435 (1997).
[2] R. M. Kerr, "Higher-order derivative correlations and the alignment of small-scale structures in isotropic numerical turbulence," J. Fluid Mech. **153**, 31 (1985).
[3] Z.-S. She, E. Jackson, and S. A. Orszag, "Intermittent vortex structures in homogeneous isotropic turbulence," Nature **344**, 226 (1990).
[4] W. T. Ashurst, A. R. Kerstein, R. M. Kerr, and C. H. Gibson, "Alignment of vorticity and scalar gradient with strain rate in simulated Navier-Stokes turbulence," Phys. Fluids **30**, 2343 (1987).
[5] M. M. Rogers and P. Moin, "The structure of the vorticity field in homogeneous turbulent flows," J. Fluid Mech. **176**, 33 (1987).
[6] J. Jiménez, "Kinematic alignment effects in turbulent flows," Phys. Fluids A **4**, 652 (1992).
[7] A. Tsinober, E. Kit, and T. Dracos, "Experimental investigation of the field of velocity gradients in turbulent flows," J. Fluid Mech. **242**, 169 (1992).
[8] A. Vincent and M. Meneguzzi, "Dynamics of vorticity tubes in homogeneous turbulence," J. Fluid Mech. **258**, 245 (1994).
[9] A. Tsinober, *An Informal Introduction to Turbulence* (Kluwer, Netherlands, 2001).
[10] B. Lüthi, A. Tsinober, and W. Kinzelbach, "Lagrangian measurement of vorticity dynamics in turbulent flow," J. Fluid Mech. **528**, 87 (2005).
[11] P. E. Hamlington, J. Schumacher, and W. J. A. Dahm, "Direct assessment of vorticity alignment with local and nonlocal strain rates in turbulent flows," Phys. Fluids **20**, 111703 (2008).
[12] G. E. Elsinga and I. Marusic, "Universal aspects of small-scale motions in turbulence," J. Fluid Mech. **662**, 514 (2010).
[13] V. Dallas and A. Alexakis, "Structures and dynamics of small scales in decaying magnetohydrodynamic turbulence," Phys. Fluids **25**, 105106 (2013).
[14] G. L. Brown and A. S. W. Thomas, "Large structure in a turbulent boundary layer," Phys. Fluids **20**, S243 (1977).
[15] C.-H. P. Chen and R. F. Blackwelder, "Large-scale motion in a turbulent boundary layer–A study using temperature contamination," J. Fluid Mech. **89**, 1 (1978).
[16] H.-P. Kreplin and H. Eckelmann, "Propagation of perturbations in the viscous sublayer and adjacent wall region," J. Fluid Mech. **95**, 305 (1979).
[17] M. R. Head and P. Bandyopadhyay, "New aspects of turbulent boundary-layer structure," J. Fluid Mech. **107**, 297 (1981).
[18] P. Moin and J. Kim, "The structure of the vorticity field in turbulent channel flow. Part 1. Analysis of instantaneous fields and statistical correlations," J. Fluid Mech. **155**, 441 (1985).
[19] A. V. Johansson, P. H. Alfredsson, and J. Kim, "Evolution and dynamics of shear-layer structures in near-wall turbulence," J. Fluid Mech. **224**, 579 (1991).
[20] M. S. Chong, A. E. Perry, and B. J. Cantwell, "A general classification of three-dimensional flow fields," Phys. Fluids A **2**, 765 (1990).
[21] H. M. Blackburn, N. N. Mansour, and B. J. Cantwell, "Topology of fine-scale motions in turbulent channel flow," J. Fluid Mech. **310**, 269 (1996).
[22] G. E. Elsinga and I. Marusic, "Evolution and lifetimes of flow topology in a turbulent boundary layer," Phys. Fluids **22**, 015102 (2010).
[23] A. Ooi, J. Martin, J. Soria, and M. S. Chong, "A study of the evolution and characteristics of the invariants of the velocity-gradient tensor in isotropic turbulence," J. Fluid Mech. **381**, 141 (1999).
[24] C. D. Meinhart and R. J. Adrian, "On the existence of uniform momentum zones in a turbulent boundary layer," Phys. Fluids **7**, 694 (1995).
[25] R. J. Adrian, C. D. Meinhart, and C. D. Tomkins, "Vortex organization in the outer region of the turbulent boundary layer," J. Fluid Mech. **422**, 1 (2000).
[26] J. C. Del Álamo, J. Jiménez, P. Zandonade, and R. D. Moser, "Self-similar vortex clusters in the turbulent logarithmic region," J. Fluid Mech. **561**, 329 (2006).
[27] S. Corrsin and A. L. Kistler, Tech. Rep. TR-1244, NACA (1955).
[28] P. Schlatter, R. Örlü, Q. Li, G. Brethouwer, J. H. M. Fransson, A. V. Johansson, P. H. Alfredsson, and D. S. Henningson, "Turbulent boundary layers up to $Re_\theta = 2500$ studied through simulation and experiment," Phys. Fluids **21**, 051702 (2009).
[29] P. Schlatter and R. Örlü, "Assessment of direct numerical simulation data of turbulent boundary layers," J. Fluid Mech. **659**, 116 (2010).
[30] S. B. Pope, *Turbulent Flows* (Cambridge University Press, 2000).